

Compared with $\alpha\text{-Fe}_2\text{O}_3$ and $\text{Zn}_x\text{Fe}_{3-x}\text{O}_4$ Thin Films Grown by Chemical Spray Pyrolysis

Sarıtaş S¹, Turgut E², Kundakci M¹, Gürbulak B^{1*} and Yildirim M¹

¹Department of Physics, Ataturk University, 25250, Erzurum, Turkey

²Department of Electrical and Energy, Aşkale Vocational School of Higher Education, Ataturk University, 25250, Erzurum, Turkey

Abstract

This work describes hematite ($\alpha\text{-Fe}_2\text{O}_3$) and $\text{Zn}_x\text{Fe}_{3-x}\text{O}_4$ thin films prepared by Chemical Spray Pyrolysis (CSP) method. CSP method allows an optimal control of stoichiometry and impurity incorporation, hematite films modified with Zn^{2+} was also prepared. Moreover, the most attracting characteristics of the hematite are its stability in neutral and basic solutions, abundance and band gap energy (2.0–2.2 eV) which permits it to absorb approximately 40% of the incident solar spectrum on earth. Nevertheless, the performance of hematite electrodes for water oxidation is restricted by their poor charge transport properties. Hematite has low conductivity and low charge-carrier mobility. In addition, the photoexcited electron-hole pairs have short life time ($\sim 10^{-12}$ s), which makes the hole diffusion length to be also short (2–4 nm). The charge transport properties of hematite can be improved by doping. We demonstrated to increase the conductivity of hematite by doping it with metal cations with 2+ charges which improved the photocatalytic properties. Doping with metal cations with 2+ charges has also brought good photoelectrochemical results. So we iron oxide and Zn-doped iron oxide compounds have been investigated.

The structural, optical and magnetic properties of $\alpha\text{-Fe}_2\text{O}_3$ and $\text{Zn}_x\text{Fe}_{3-x}\text{O}_4$ compounds have been extensively investigated. XRD, XPS, Raman, FE-SEM and AFM techniques have been used for structural analysis; Absorption technique has been used for optical properties; Hall and Vibrating Sample Magnetometer (VSM) techniques have been used for magnetic properties.

Keywords: Hematite; Zn-doped iron oxide; Photoelectrochemical (PEC); Thin film

Introduction

Photocatalysis has been attracting much research interest because of its wide applications in renewable energy and environmental restoration; however materials limitations have significantly hindered their efficiency. Researchers to find different techniques to use solar energy as an alternative for future energy needs. The objective of our research is to improve the efficiencies of PEC cells by identifying and engineering corrosion-resistant semiconductors that exhibit the optimal conduction and valence band edge alignment for PEC applications [1,2]. There are many materials that are found to show good photocatalytic activity in the presence of Ultraviolet (UV) and visible light. The most common method to directly convert solar energy into electric energy is Photovoltaic (PV), and this process utilizes semiconductors which generate electron-hole pairs upon illumination with visible light, thereby producing electric power in solar cells. However, the utility of photovoltaic cells is limited by poor conversion efficiency. To overcome these problems, researchers have tried to find suitable methods to produce hydrogen (H_2) from photocatalysis of H_2O using sunlight, which can be used in fuel cells for power generation. However, the applications of these materials are limited to the UV portion of sunlight. $\alpha\text{-Fe}_2\text{O}_3$ has an advantage over the other conventional materials like TiO_2 , ZnO , WO_3 etc. in using solar energy for photocatalytic applications due to its lower band gap ~ 2.2 eV value. As a result of which Fe_2O_3 is capable of absorbing a large portion of the visible solar spectrum (absorbance edge ~ 600 nm). Also its good chemical stability in aqueous medium, low cost, abundance and nontoxic nature makes it a promising material for photocatalytic water treatment and water splitting applications [3].

However, the photocatalytic performance of $\alpha\text{-Fe}_2\text{O}_3$ is limited by certain factors such as high recombination rate of electrons and holes, low diffusion lengths of holes (2–4 nm). And poor conductivity, which led to both low efficiencies and a larger requisite over potential for photo-assisted water oxidation [4-8]. Many attempts have been made

by researchers to overcome these anomalies of $\alpha\text{-Fe}_2\text{O}_3$ such as lowering the recombination rate by forming nanostructures, enhancement in conductivity by doping with suitable metals and improving the charge transfer ability [9,10].

Photocatalytic ability in materials is one of the most interesting research topics due to its usefulness in various fields such as H_2 generation [11-13], artificial photosynthesis [14,15], waste water treatment [16-18], removal of toxic gases from air [19-21].

Fossil fuels have been the most consumed energy by the World during the last 40 years. Indeed, fossil fuels provided approximately 87% of global energy consumption in 2013. Using this kind of energy will continue to provoke the emission of greenhouse gases (e.g. CO_2) that pollute and damage our environment. Therefore, optimizing the technology of clean and renewable energies is urgent in order to diminish the use of fossil fuels, and, thus, it will permit the preservation of our environment for the next generations [22-27].

Spintronics is another application field of technology for Iron Oxide, whereas conventional electronic devices ignore the spin property and rely strictly on the transport of the electrical charge of electrons. Spintronics is an emergent nano technology which deals with spin dependent properties of an electron instead of or in addition to its charge dependent properties. Adding the spin degree of

*Corresponding author: Gürbulak B, Department of Physics, Ataturk University, 25250, Erzurum, Turkey, Tel: +90 442 231 4177; E-mail: gurbulak@atauni.edu.tr

Received June 11, 2017; Accepted July 04, 2017; Published July 11, 2017

Citation: Sarıtaş S, Turgut E, Kundakci M, Gürbulak B, Yildirim M (2017) Compared with $\alpha\text{-Fe}_2\text{O}_3$ and $\text{Zn}_x\text{Fe}_{3-x}\text{O}_4$ Thin Films Grown by Chemical Spray Pyrolysis. Int J Sens Netw Data Commun 6: 152. doi: 10.4172/2090-4886.1000152

Copyright: © 2017 Sarıtaş S, et al. This is an open-access article distributed under the terms of the Creative Commons Attribution License, which permits unrestricted use, distribution, and reproduction in any medium, provided the original author and source are credited.

freedom provides new effects, new capabilities and new functionalities. Spintronic devices offer the possibility of enhanced functionality, higher speed, and reduced power consumption. High-volume information-processing and communications devices are at present based on semiconductor devices, whereas information-storage devices rely on multilayers of magnetic metals and insulators. Spin transistors would allow control of the spin current in the same manner that conventional transistors can switch charge currents, which was first spin device proposed for metal-oxide geometry [28-30].

Experimental Details

CSP is one of the solution based coating technique to produce metallic and semiconductor thin or thick films. Apart from the many other thin film fabrication methods, this technique is quite simple and comparatively cost effective. Dense, porous or multi-layered films in any composition can be fabricated using this versatile method. Temperature control unit, substrate heater, deposition solution and atomizer are components of the CSP setup. Different type of atomizers such as air blast, ultrasonic or electrostatic can be employed depending on properties of liquid and operating conditions to obtain coatings with desired properties. Atomized droplets of deposition solution spread over the surface of the substrates with respect to the temperature of substrate, volume and momentum of the droplets. The interaction of droplets with substrate surface, aerosol transport, and evaporation of solvent and decomposition of precursor are consecutive or simultaneous processes of this processing technique and these processes are accompanied by decomposition temperature. Therefore, temperature is the main parameter of CSP and significantly affects the microstructural, optical and electrical properties of the resultant thin film. Moreover, air flow rate, nozzle distance and viscosity of deposition solution are the other controllable processing parameter to produce high quality coatings. The salts given in Table 1 were prepared as 0.1 molar solutions in deionized water. The substrate was sprayed with argon gas onto a substrate heated to 320°C at a distance of 30 cm [30-34].

Results and Discussion

The structural, optical and magnetic properties of a-Fe₂O₃ and Zn_xFe_{3-x}O₄ compounds have been extensively investigated. XRD, XPS, Raman, FE-SEM and AFM techniques have been used for structural analysis; Absorption technique has been used for optical properties; Hall and Vibrating Sample Magnetometer (VSM) techniques have been used for magnetic properties.

The XRD diffraction pattern of the iron oxide structure growing on the glass substrate is given in Figure 1 and it has been determined that the structure has a tetragonal structure (Table 2). The lattice constants a=b=8.33 Å, c=24.99 Å. Four evident peaks are observed, of which characteristic hematite peak is observed at 32.30 degrees.

In Figure 1, XRD diffraction patterns of Fe₂O₃ and Zn_xFe_{3-x}O₄ thin films are given. As can be seen from this figure, when compared with the Zn_xFe_{3-x}O₄ structure of the Fe₂O₃ structure, the XRD peaks are narrower and more intense, while the peaks of the newly formed structure are observed and the resulting structure is polycrystalline (Table 3).

In Figure 2 the value of the energy of the band gap is calculated 2.16 eV, 2.14 eV with the fit drawn on the energy graph against the (ahv)² (cm⁻¹ eV²) of the Fe₂O₃, Zn_xFe_{3-x}O₄ thin films grown by CSP technique, respectively. As Fe₂O₃ thin film gives absorption at smaller wave lengths, it shifts at larger wave length as a result of doping (Table 4). This may mean that the energy band gap is causing the contraction of the band gap due to the fact that the imperfections in the structure constitute the possibility of transition at the band edge [35,36].

Figure 3 shows the Raman shift of the stretching vibration mode of Fe₂O₃ films are seen. There are Raman active states of the hematite phase that these peaks are relatively narrow and severe. In the Zn_xFe_{3-x}O₄ compound, the peak of the Raman shift peaks belonging to the hematite phase falls. In addition, the peaks showing the ramping changes of the stretching vibration mode of the Zn_xFe_{3-x}O₄ film is due to the presence of multiple phases due to polycrystalline crystal structure [31].

XPS is used for the analysis of the elemental and chemical state information of the investigated surfaces and can be made approximately 10 nm from the surface. It is able to detect the ions and ligand energies attached to the chemical ligands of the sample studied.

As shown in Figure 4a; Tables 5 and 6 the binding energy of the 2p_{3/2}, 2p_{1/2} orbitals for the Fe³⁺ (Fe₂O₃) ion are 711 and 724 eV, respectively. The 1s orbital binding energy of the O²⁻ ion is 531 eV. The peak intensities of the connecting electrons are very close to one another and the number of non-bonding electrons is small, which can be seen as the reason for the insulating properties [37].

We can also say that the conductivity is low because the atomic percentage of the oxygen atom is 65.96% (Table 6) and the oxygen vacancies causing the conductivity are low.

As can be seen in Figure 4b; Tables 5 and 6 the graph showing the binding energies of the Fe³⁺, Zn²⁺ and O²⁻ ions of the Zn_xFe_{3-x}O₄ composition is almost identical to the atomic oxygen content of the Fe₂O₃ compound, There has been no drop in severity. It is believed that

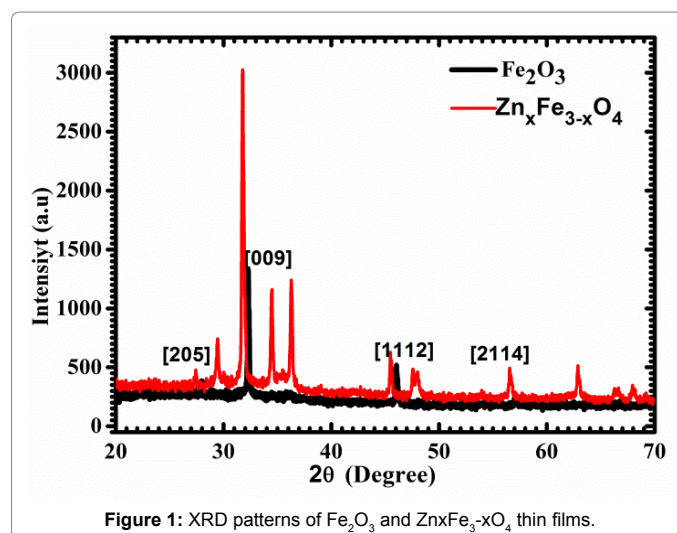


Figure 1: XRD patterns of Fe₂O₃ and Zn_xFe_{3-x}O₄ thin films.

Film	Used Chemical Salt	Solution Molar Ratio	Substrate Temperature (°C)	Carrier Gas	Grown Time (min)
Fe ₂ O ₃	FeCl ₃ ·6H ₂ O+FeCl ₂ ·4H ₂ O+NaOH	02:00:2	320	Argon	35
Zn _x Fe _{3-x} O ₄	FeCl ₃ ·6H ₂ O+FeCl ₂ ·4H ₂ O+NaOH+Zn(NO ₃) ₂ ·6H ₂ O	1:2:0.25:0.1:0.01	320	Argon	35

Table 1: Experimental details of the Fe₂O₃ and Zn_xFe_{3-x}O₄ thin films grown by chemical spray pyrolysis technique.

2θ°	(hkl)	FWHM	Lattice Constant	d (Å)	Crystal System	Chemical Formula	Reference Code
28,14	205	0.071	a=b=8,33 c=24,99	3,21	Tetragonal	Fe ₂ O ₃	00-015-0615
32,30	9	0.437	a=b=8,33 c=24,99	2,79	Tetragonal	Fe ₂ O ₃	00-015-0615
46,02	1112	0.174	a=b=8,33 c=24,99	1,94	Tetragonal	Fe ₂ O ₃	00-015-0615
57,02	2114	0.001	a=b=8,33 c=24,99	1,60	Tetragonal	Fe ₂ O ₃	00-015-0615

Table 2: Structural properties obtained from XRD patterns of Fe₂O₃ thin film.

2θ°	(hkl)	FWHM	d (Å)	Crystal system	Chemical formula	Lattice constant	Reference Code
27,45	15	0,150	3,24	Hexagonal	Fe ₂ O ₃	a=5,560 b=5,560 c=22,550	01-076-1821
29,44	7	0,135	3,03	Hexagonal	Fe ₂ O ₃	a=5,560 b=5,560 c=22,550	01-076-1821
31,77	220	0,171	2,81	Cubic	ZnFe ₂ O ₄	a=b=c=8,30	01-073-1963
34,50	311	0,001	2,59	Cubic	ZnFe ₂ O ₄	a=b=c=8,44	01-086-0507
36,28	222	0,191	2,47	Cubic	ZnFe ₂ O ₄	a=b=c=8,30	01-073-1963
45,49	249	0,100	1,99	Hexagonal	ZnFe ₂ O ₄	a=12,80 b=12,80 c=57,26	00-045-1186
47,60	331	0,001	1,91	Cubic	ZnFe ₂ O ₄	a=b=c=8,30	00-016-0653
47,97	331	0,262	1,89	Cubic	ZnFe ₂ O ₄	a=b=c=8,30	00-016-0653
56,57	511	0,148	1,62	Cubic	ZnFe ₂ O ₄	a=b=c=8,30	00-016-0653
62,86	440	0,001	1,47	Cubic	ZnFe ₂ O ₄	a=b=c=8,35	01-073-1963
66,54	531	0,090	1,40	Cubic	ZnFe ₂ O ₄	a=b=c=8,35	01-073-1963
68,02	22-Mar	0,090	1,37	Hexagonal	Fe ₂ O ₃	a=5,560 b=5,560 c=22,550	01-076-1821

Table 3: Structural properties obtained from XRD patterns of Zn_xFe_{3-x}O₄ thin film.

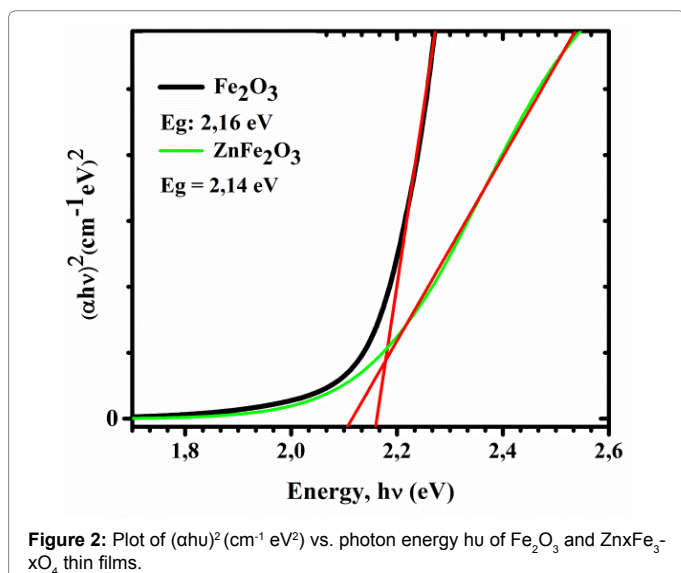


Figure 2: Plot of $(\alpha h\nu)^2$ ($\text{cm}^{-1} \text{eV}^2$) vs. photon energy $h\nu$ of Fe₂O₃ and Zn_xFe_{3-x}O₄ thin films.

this may be due to the fact that some of the Zn may have been linked to O, such that the Zn is linked to the Fe₂O₃ compound.

It is known that Zn is alloyed with Fe, and as it is known, when an alloy occurs, it often occurs that an element has a defect in the structure of the other element. It can be said that the decrease of Fe in the Zn_xFe_{3-x}O₄

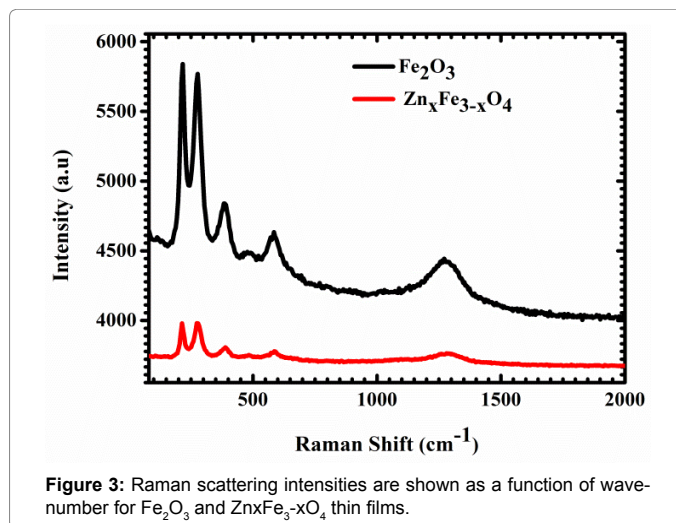


Figure 3: Raman scattering intensities are shown as a function of wave-number for Fe₂O₃ and Zn_xFe_{3-x}O₄ thin films.

Elements	Raman Shift (cm)	Mod
Fe ₂ O ₃	216;277; 216;277	Hematit; [(A1g) 225], [(Eg) 249],[(Eg) 295],[(Eg) 302]
Zn _x Fe _{3-x} O ₄	212;274;384; 212;274;384	Zinc ferrit [F2g(2) 355] [F2g(3) 451] [26-28]

Table 4: Raman shift and modes of Fe₂O₃ ve Zn_xFe_{3-x}O₄ thin films.

xO₄ compound in Fe₂O₃ compound is due to the Zn incorporated in the structure. This also supports XRD results. For the Fe³⁺ (Fe₂O₃) ion, the binding energy of the 2p 3/2, 2p1/2 orbitals is 711.65 eV and 724.3 eV, respectively. The 1s orbital binding energy of the O²⁻ ion is 530 eV. The binding energy for 2p3/2 and 2p1/2 orbitals for Zn²⁺ ion is 1024.23 and 1047.98 eV, respectively. If we think that the reduction in the amount of binding oxygen can be interpreted as oxygen vacancies in the structure, the cause of the increase in conductance will become apparent.

In Figure 5a, the pure Fe₂O₃ compound was given a 200 nm scaled FE-SEM image at about 171,000 magnifications taken at 6.6 mm working distance with an inlens detector. As can be seen from this figure, it can be said that the surface/volume ratio in which a stacked leaf-like image exists, it is a widely used material for gas sensor application [29]. Also films surface cover with OH⁻¹ groups.

Figure 5b shows FE-SEM images of the Zn_xFe_{3-x}O₄ compound at 400,000 magnifications. It is possible to say that the composition is homogeneously dispersed on the surface and that there is a nano porous structure. However, it was found that the decrease of the nanoporous structure in the Zn_xFe_{3-x}O₄ compound films grown by adding the solution of zinc nitrate solution prepared for the Fe₂O₃ thin film was confirmed that the Zn element was mixed more into the structure and the pores were closed. This nano porous structure can be used as a suitable substrate for forming many nano rod structures.

Figure 6 shows two-dimensional and three-dimensional (5 × 5 μm) AFM images of Fe₂O₃ thin film. As it can be seen, there are locally pebbles, and circular-like clusters are arranged regularly. The roughness value is about 28 nm with a maximum height of 51 nm and a maximum depth of 79 nm. The average roughness value Rq\RMS value is 33 nm, which is almost consistent with the linear roughness value.

In Figure 7, the two-dimensional and three-dimensional (5 × 5 μm) AFM images obtained for the Zn_xFe_{3-x}O₄ film showed that the particles in the structure showed a sharper image. There are pits and hills almost

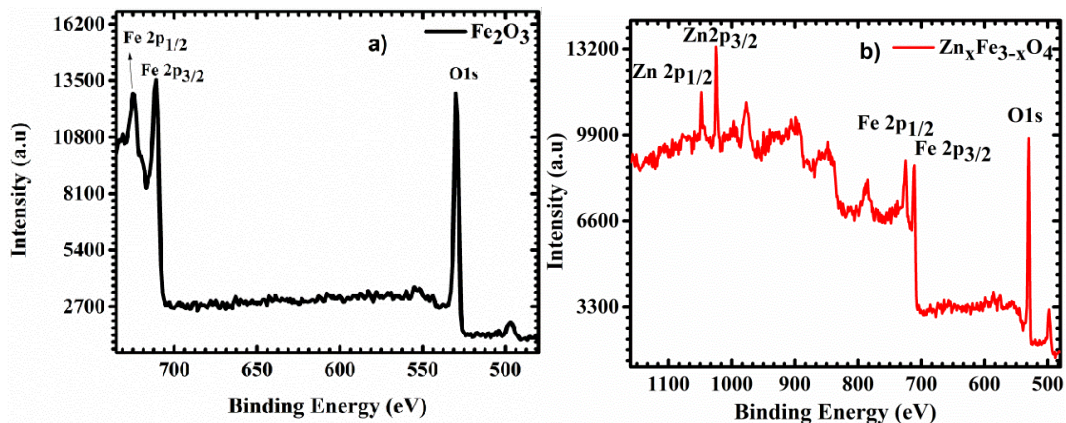


Figure 4: XPS analysis of a) Fe₂O₃ and b) Zn_xFe_{3-x}O₄ thin films.

Elements	Experimental Ion Binding Energy (eV)		Literature Ion Binding energy (eV)		
	2p _{1/2}	2p _{3/2}	Ion	2p _{1/2}	2p _{3/2}
Fe	724,30	711,65	Fe ³⁺ (Fe ₂ O ₃)	724,30	710,70
Zn	1047,98	1024,23	Zn ²⁺ (ZnO)	1044,7	1021,70

Table 5: XPS measurement results of the binding energy according to orbitals of Fe³⁺, Zn²⁺ ions.

Compound	Orbital	Intensity	% Atomic
Fe ₂ O ₃	O 1s	12969	65.96
	Fe 2p _{3/2}	13470	34.04
Zn _x Fe _{3-x} O ₄	O 1s	9847	67.39
	Fe 2p _{3/2}	8718	27.93
	Zn 2p _{3/2}	13377	4.67

Table 6: The atomic percentage of the elements in the structure, orbital, peak intensity, bound by ions in the compounds.

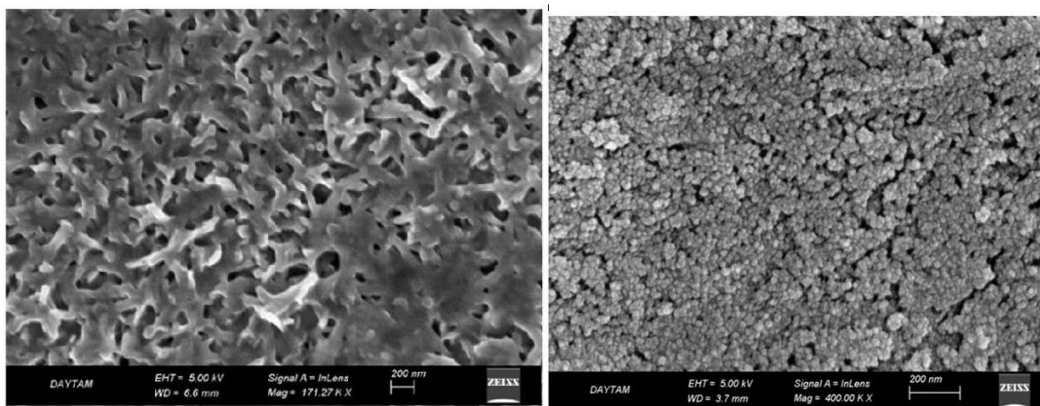


Figure 5: FE-SEM images of (a) Fe₂O₃ and (b) Zn_xFe_{3-x}O₄.

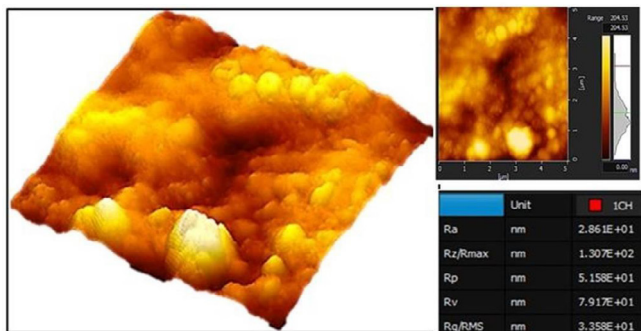


Figure 6: AFM images of the Fe₂O₃ thin film (Average height is 270.1 nm).

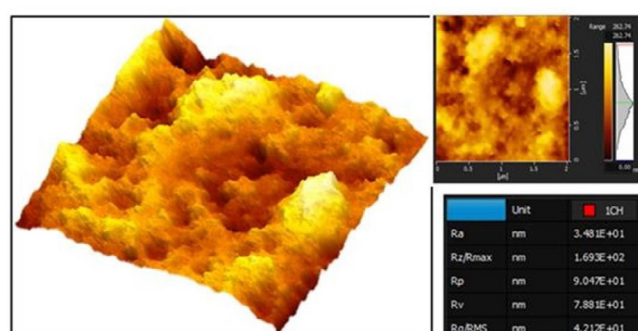


Figure 7: AFM images of the Zn_xFe_{3-x}O₄ thin film (Average height is 266.6 nm).

everywhere resembling craters. The roughness value is about 34 nm, with a maximum height of 90 nm and a maximum depth of 78 nm. The average roughness value Rq\RMS value is 41 nm, which is almost in line with the linear roughness value. The variability of the colors tone indicates that the height difference in the topography is great. It is possible to say that the surface consists mostly of hills and pits.

Figure 8 shows that the sharp morphology of the Zn_xFe_{3-x}O₄ thin-film AFM image in the three-dimensional (5 × 5 μm) AFM image of Zn_xFe_{3-x}O₄ with a magnification of 5 min resulted in a large structure of sharp-pointed surface area and that the existing morphology stood out as shown in Figure 8. Here, a large surface area appears to be formed and the roughness value is 2.2 nm. It can be considered that such less rough Zn_xFe_{3-x}O₄ thin films are an ideal material for gas sensor application [30].

Results of Hall measurement of p-type Fe₂O₃ thin film are considered, it is expected that the carriers in the valence band of the semiconductor materials may pass to the acceptor levels by thermal excitation and contribute to the conductivity (Figure 9a). In the enlarged film the carrier density is reduced and the resistivity is increased. We can say that the holes in the valence band of the p-type semiconducting material are compensated by the donor type defects and impurities and therefore the density of the hole carrier is lowered (Figure 9b). In this case, the decrease in Hall mobility due to the increased temperature is consistent with the literature (Figure 10a). Phonon scattering of the carriers becomes predominant as temperature increases the vibration amplitude of the cage ions. This may result in an average free path reduction.

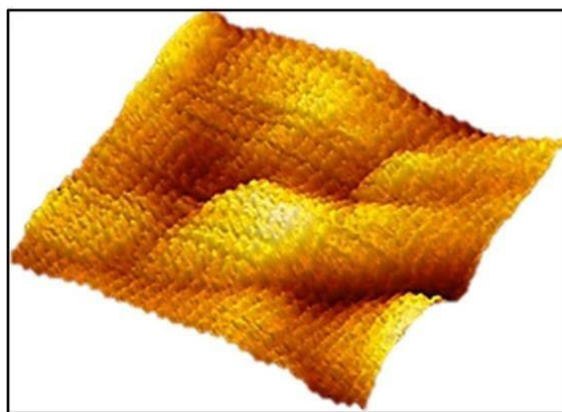


Figure 8: AFM images of the Zn_xFe_{3-x}O₄ thin film (5 min grown, average height is 17.5 nm).

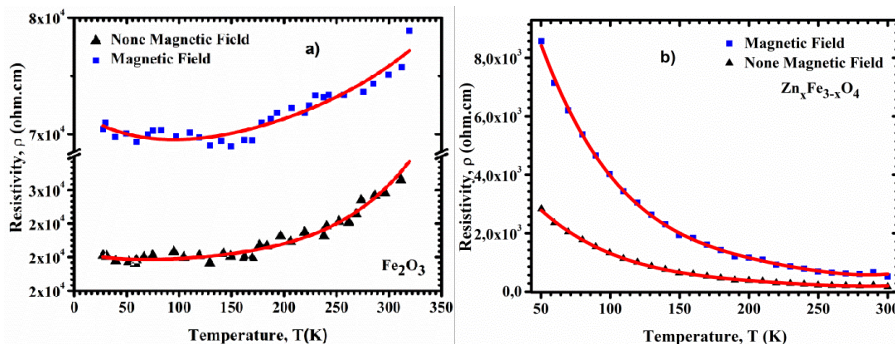


Figure 9: Resistivity versus temperature for (a) a-Fe₂O₃ and (b) Zn_xFe_{3-x}O₄.

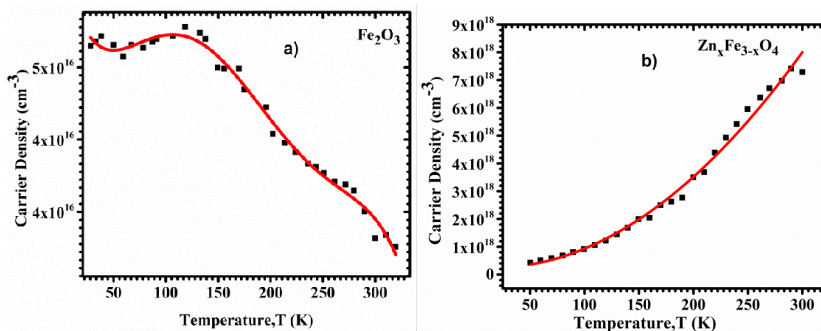


Figure 10: Carrier density versus temperature for (a) a-Fe₂O₃ and (b) Zn_xFe_{3-x}O₄.

As can be seen in Figure 10b it is seen that the p-type Zn_xFe_{3-x}O₄ semiconducting compound exhibits a semiconductor character in the result of the increase in the temperature (50-300 K). Due to the increased temperature the resistivity decreases. In addition, the magnetic field increases the resistivity of the material and shows a positive magneto resistance effect. We can say that the results obtained are in the expected direction and agree with each other.

Figure 10b shows the increase in carrier density due to the increasing temperature of p-type Zn_xFe_{3-x}O₄ thin film. The increase in the number of whole carriers in the valence band with p-type semiconductor-induced thermal excitation can be seen under normal conditions.

Figure 11a and 11b shows the decrease in Hall mobility due to the increased temperature of Zn_xFe_{3-x}O₄ thin films. As a result, the carrier density has increased by two orders of magnitude.

In Figure 12a, the magnetic hysteresis curve of the Fe₂O₃ thin film is observed to be relatively narrow. The saturation magnetic torque value is 4.4×10^{-5} emu, which corresponds to a value of 15.78 Oe. In addition, the coercive force is -0.66 Oe and the remanence magnetic moment is 0.74. It has an emu value of 10^{-5} . In these values, it has been determined that Fe₂O₃ has a soft magnetic property. Soft magnetic materials are used in devices that are exposed to alternative magnetic fields and therefore must have low energy losses. They are commonly used in transformers, electric motors, generators, dynamo and switch circuits.

In Figure 12b, the magnetic hysteresis curve of Zn_xFe_{3-x}O₄ thin film seems to be relatively wide. The saturation magnetic moment value is $3.94 \cdot 10^{-5}$ emu, which corresponds to 1.72 kOe. The coercive force is

-2.98 kOe and the remanence magnetic moment is 3.31. It has an emu value of 10^{-5} . When the hysteresis curve is taken into consideration, it can be said that the material exhibits hard magnetism and is difficult to demagnetize. One of the most important application areas of hard magnetic materials is motors. In addition, hard magnets are preferred in wireless drills, screwdrivers, automobile windshield wipers, water sprayers, contact circuits, ventilation systems, recorders, clocks. Other applications that benefit from hard magnets include speakers, headphones, and computer hardware in the audio system.

Conclusion

Undoped and modified with Zn²⁺ hematite films were synthesized by the CSP method at 320°C temperature. Raman shifts (216 cm⁻¹, 277 cm⁻¹, 383 cm⁻¹, 584 cm⁻¹, 1272 cm⁻¹) of the stretching vibration mode of Fe₂O₃ films are seen. There are Raman active states of the hematite phase that these peaks are relatively narrow and severe. In the Zn_xFe_{3-x}O₄ compound, the peak of the Raman shift peaks belonging to the hematite phase falls. In addition, the peaks showing the ramping changes of the stretching vibration mode of the Zn_xFe_{3-x}O₄ film is due to the presence of multiple phases due to polycrystalline crystal structure and this is consistent with XRD results.

It was demonstrated that the Zn²⁺ doped influenced on the photocatalytic performance of films. The Zn²⁺ doped hematite film exhibited a better photocatalytic performance than undoped hematite film. Hematite has low conductivity and low charge-carrier mobility. In addition, the photoexcited electron-hole pairs have short life time ($\sim 10^{-12}$ s), which makes the hole diffusion length to be also short (2-4 nm). The charge transport properties of hematite can be improved by doping. The better performance of Zn²⁺ doped film was attributed to

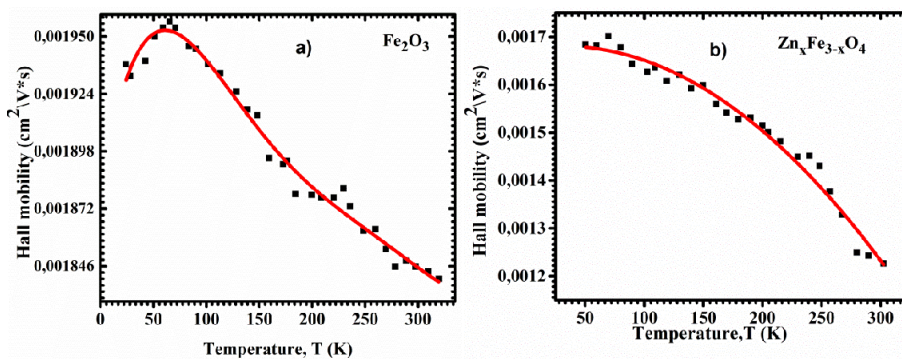


Figure 11: Hall Mobility versus temperature for (a) a-Fe₂O₃ and (b) Zn_xFe_{3-x}O₄.

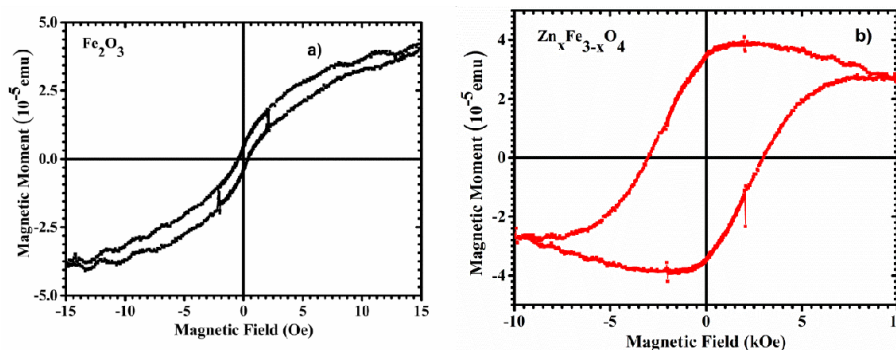


Figure 12: M-H curves for (a) Fe₂O₃ and (b) Zn_xFe_{3-x}O₄ thin films.

their higher carrier density that improved their conductivity. Because the carrier concentration of Zn_xFe_{3-x}O₄ is 7.2×10^{18} and the carrier concentration of Fe₂O₃ is 4.2×10^{16} . So the carrier concentration of Zn_xFe_{3-x}O₄ is nearly 10^2 times greater. When we consider the magnetization situation, the hardest magnetization property is Zn_xFe_{3-x}O₄ film that the magnetic hysteresis curve of Zn_xFe_{3-x}O₄ thin film seems to be relatively wide. The saturation magnetic moment value is $3.94 \cdot 10^{-5}$ emu, which corresponds to 1.72 kOe, the softest magnetization feature is Fe₂O₃ film that the magnetic hysteresis curve of the Fe₂O₃ thin film is observed to be relatively narrow. The saturation magnetic torque value is $4.41 \cdot 10^{-5}$ emu, which corresponds to a value of 15.78 Oe. It can be said here that Zn, which has no magnetic property, causes pinning which make defects in the structure difficult to move the domains.

Also when we evaluate the films grown using CSP technique in terms of their applications; Fe₂O₃ and Zn_xFe_{3-x}O₄ films are suitable for spintronic applications. Spintronics is an emergent nano technology which deals with spin dependent properties of an electron instead of or in addition to its charge dependent properties. We can see in the results of VSM that the Fe₂O₃ compound can control its magnetic properties by doping with Zn. As a result controlling magnetic properties is very important for spin transistor applications.

References

- Hoseinzadeh S, Ghasemiasl R, Bahari A, Ramezani AH (2017) The injection of Ag nanoparticles on surface of WO₃ thin film: Enhanced electrochromic coloration efficiency and switching response. *Journal of Materials Science: Materials in Electronics* (In Publish).
- Hoseinzadeh S, Ghasemiasl R, Bahari A, Ramezani AH (2017) n-type WO₃ semiconductor as a cathode electrochromic material for ECD devices. *Journal of Materials Science: Materials in Electronics* (In Publish).
- Mishra M, Chun DM (2015) α -Fe₂O₃ as a photocatalytic material: A review. *Applied Catalysis A: General* 498: 126-141.
- Sartoretti CJ, Ulmann M, Alexander BD, Augustynski J, Weidenkaff A (2003) Photoelectrochemical oxidation of water at transparent ferric oxide film electrodes. *Chem Phys Lett* 376: 194-200.
- Kennedy HJ, Frese WKJ (1978) Photo oxidation of water at α -Fe₂O₃ electrodes. *J Electrochem Soc* 125: 709-714.
- Morin JF (1951) Electrical properties of α -Fe₂O₃ and α -Fe₂O₃ containing titanium. *Phys Rev* 83: 1005-1010.
- Morin JF (1954) Electrical properties of α -Fe₂O₃. *Phys Rev* 93: 1195-1199.
- Dare-Edwards PM, Goodenough BJ, Hamnett A, Trevellick RP (1983) Electrochemistry and photoelectrochemistry of iron(III) oxide. *J Chem Soc Faraday Trans* 79: 2027-2041.
- Sivula K, Formal LF, Grätzel M (2011) Solar Water Splitting: Progress Using Hematite (α -Fe₂O₃) Photoelectrodes. *Chem Sus Chem* 4: 432-449.
- Katz JM, Riha SC, Jeong NC, Martinson ABF, Farha OK, et al. (2012) Toward solar fuels: Water splitting with sunlight and "rust"? *Coord Chem Rev* 256: 2521-2529.
- Barroso M, Mesa CA, Pendlebury SR, Cowan AJ, Hisatomi T, et al. (2012) Dynamics of photogenerated holes in surface modified α -Fe₂O₃ photoanodes for solar water splitting. *PNAS* 109: 15640-15645.
- Ni M, Leung MKH, Leung DY, Sumathy K (2007) A review and recent developments in photocatalytic water-splitting using TiO₂ for hydrogen production. *Renew Sustain Energy Rev* 11: 401-425.
- Maeda K, Domen K (2007) New Non-Oxide Photocatalysts Designed for Overall Water Splitting under Visible Light. *J Phys Chem C* 111: 7851-7861.
- Concepcion JJ, House RL, Papanikolas JM, Meyer TJ (2012) Chemical approaches to artificial photosynthesis. *PNAS* 109: 15560-15564.
- Bora DK, Hu Y, Thiess S, Erat S, Feng X, et al. (2013) Between photocatalysis and photosynthesis: Synchrotron spectroscopy methods on molecules and materials for solar hydrogen generation. *J Electron Spectrosc* 190: 93-105.
- Sun S, Wang W, Zeng S, Shang M, Zhang L (2010) Preparation of ordered mesoporous Ag/WO₃ and its highly efficient degradation of acetaldehyde under visible-light irradiation. *J Hazard Mater* 178: 427-433.
- Arabatzi IM, Stergiopoulos T, Andreeva D, Kitova S, Neophytides SG, et al. (2003) Characterization and photocatalytic activity of Au/TiO₂ thin films for azo-dye degradation. *J Catal* 220: 127-135.
- Sonawane RS, Dongare MK (2006) Sol-gel synthesis of Au/TiO₂ thin films for photocatalytic degradation of phenol in sunlight. *J Mol Catal A: Chem* 243: 68-76.
- Lin L, Chai Y, Zhao B, Wei W, He D, et al. (2013) Photocatalytic oxidation for degradation of VOCs. *Open J Inorg Chem* 3: 14-25.
- Mo J, Zhang Y, Xu Q, Joaquin Lamson J, Zhao R (2009) Photocatalytic purification of volatile organic compounds in indoor air: A literature review. *Atmos Environ* 43: 2229-2246.
- Wang W, Soulis J, Yang YJ, Biswas P (2014) Comparison of CO₂ photoreduction systems: A review". *Aerosol Air Qual Res* 14: 533-549.
- Gasparov LV, Tanner DB, Romero DB, Berger H, Margaritondo G, et al. (2000) Infrared and Raman studies of the verwey transition in magnetite. *Phys Rev B: Condens Matter Mater Phys* 62: 7939-7944.
- Chamritski I, Burns G (2005) Infrared-and Raman-active phonons of magnetite, maghemite, and hematite: a computer simulation and spectroscopic study. *J Phys Chem B* 109: 4965-4968.
- Bersani D, Lottici PP, Montenero A (1999) Micro-Raman investigation of iron oxide films and powders produced by sol-gel syntheses. *J Raman Spectrosc* 30: 355-360.
- Jubb AM, Allen HC (2010) Vibrational spectroscopic characterization of hematite, maghemite, and magnetite thin films produced by vapor deposition applied materials and interface. *ACS Appl Mat Inter* 2: 2804-2812.
- Singh JP, Srivastava RC, Agrawal HM, Kumar R (2011) Micro-Raman investigation of nanosized zinc ferrite: effect of crystallite size and fluence of irradiation. *J RAMAN Spectrosc* 42: 1510-1517.
- De Faria DLA, Silva SV, De Oliveira MT (1997) Raman microspectroscopy of some iron oxides and oxyhydroxides. *J Raman Spectrosc* 28: 873-878.
- Rivero M, Del CA, Mayoral A, Mazario E, Sanchez-Marcos J, et al. (2016) Synthesis and structural characterization of Zn_xFe_{3-x}O₄ ferrite nanoparticles obtained by an electrochemical method. *RSC Adv* 6: 40067-40076.
- Pawar NK, Kajale DD, Patil GE, Wagh VG, Gaikwad VB, et al. (2012) Nanostructured Fe₂O₃ thick film as an ethanol sensor. *International Journal on Smart Sensing and Intelligent Systems* 5: 441-457.
- Yuan HL, Liu E, Yin YL, Zhang W, Wong PKJ, et al. (2016) Enhancement of magnetic moment in Zn_xFe_{3-x}O₄ thin films with dilute Zn substitution. *Appl Phys Lett* 108: 232403.
- Bellido-Aguilar DA, Tofanello A, Souza FL, Furini LN, Constantino CJL (2016) Effect of thermal treatment on solid-solid interface of hematite thin film synthesized by spin-coating deposition solution. *Thin Solid Films* 604: 28-39.
- I.E. AGENCY (2013) Key world energy statistics.
- BP Company (2014) BP statistical review of world energy.
- Solangi KH, Islam MR, Saidur R, Rahim NA, Fayaz H (2011) A review on global solar energy policy. *Renew Sustain Energy Rev* 15: 2149-2163.
- Van De Krol R, Gratzel M (2012) Photoelectrochemical hydrogen production. Springer Science.
- Wang Z, Roberts RR, Naterer GF, Gabriel KS (2012) Comparison of thermochemical, electrolytic, photoelectrolytic and photochemical solar-to-hydrogen production Technologies. *Int J Hydrogen Energy* 37: 16287-16301.
- Dincer I (2012) Green methods for hydrogen production. *Int J Hydrogen Energy* 37: 1954-1971.